EurJIC
European Journal of Inorganic Chemistry

Full Papers
doi.org/10.1002/ejic.202000941

Chemistry Europe
European Chemical Societies Publishing

Direct Assessment of Ultralow Li^+ Jump Rates in Single Crystalline Li_3N by Evolution-Time-Resolved ^7Li Spin-Alignment Echo NMR

Bernhard Gadermaier,[a] Katharina Hogrefe,[a] Paul Heitjans,[b] and H. Martin R. Wilkening*[a]

Diffusion processes of small cations and anions play important roles in many applications such as batteries and sensors. Despite the enormous progress we have witnessed over the past years in characterizing the irregular movement of ions such as Li^+, new methods able to sharpen our view and understanding of fast and slow diffusion phenomena are steadily developed. Still, very few techniques are, however, available to directly sense extremely slow Li^+ diffusion processes. Here, we took advantage of 1D evolution-time resolved ^7Li spin-alignment echo NMR that is able to probe the extremely slow interlayer Li^+ hopping process in layer-structured Li_3N, which served as a model substance for our purposes. The use of single crystals enabled us to study this translational process without being interfered by the fast intralayer Li^+ motions. At 318 K the corresponding jump rate of interlayer dynamics turned out to be in the order of 2500(200) s^{-1} resulting in a diffusion coefficient as low as 1×10^{-17} $m^2 s^{-1}$, which is in excellent agreement with results from literature. The method, comparable to 1D and 2D NMR exchange spectroscopy, relies on temporal fluctuations of electric interactions the jumping ions are subjected to. ^7Li single crystal 1D SAE NMR offers new opportunities to precisely quantify slow Li^+ diffusion processes needed to validate theoretical models and to develop design principles for new solid electrolytes.

Introduction

The binary compound lithium nitride, Li_3N, is one of the most fascinating Li^+ ion conductors ever studied.[1] It experienced its golden period, considering studies focusing on ionic transport, during the 70s when researchers, especially those at the Max-Planck Institute for Solid State Research in Stuttgart, started working with Li_3N single crystals.[1e,f,h,2] Such crystals, grown by the Czochralski method, are ruby red revealing the typical habit of a layer-structured crystal (see Figure 1).

In Figure 1 the α-modification of Li_3N (space group *P6/mmm*) is depicted with its two magnetically and electrically inequivalent Li sites, here denoted as Li(1) and Li(2). Li_3N can be described as a sequence of Li and Li_2N layers perpendicular to the c-axis.[1f,2a] N atoms occupy the center of the unit cell and are surrounded by 8 Li atoms in the form of a hexagonal bipyramid. Orientation dependent optical absorption experiments revealed an indirect band gap of 2.05 to 2.2 eV (300 K to 4.2 K).[1f] The intensity of an absorbent shoulder in the long-wavelength region depends on the concentration of intrinsic defects.[1f] Hydrogen incorporation belongs to one of the most important extrinsic defects in Li_3N affecting the intralayer diffusion process;[3] a weak Li–N bond next to an NH^{2-} group was proposed to facilitate Li^+ Frenkel defect formation and vacancy migration.[4]

Whereas fast Li^+ exchange occurs within the Li-rich nitrogen layers[1e,2a,5] (the Li(2)-Li(2′) distance $d_{22'}$ is approximately 2 Å), hopping processes perpendicular to the ab-plane are much less frequent ($d_{12} = 2.86$ Å).[1a–f,h,i,2a,5a–c,6] The (axially symmetric)[7] electric field gradients (EFGs) at the nuclear sites of Li(1) and Li(2) in Li_3N greatly differ in magnitude.[1b,i,6–8] Thus, the corresponding ^7Li (spin-quantum number $I = 3/2$) nuclear magnetic resonance spectrum of Li_3N is, at room temperature, composed of two distinct pairs of satellite lines flanking the Li(1) and Li(2) central transitions, see Figure 1a.[9] The positions of the central lines on the frequency scale are influenced by 2nd order quadrupolar interactions (Figure 1a, inset).[1b,h] The corresponding satellite lines are marked with asterisks and dots in Figure 2a, this assignment takes into account the fact that the two EFGs differ in (algebraic) sign.[1h,i,7,10]

The ^7Li NMR spectrum of Li_3N, which is the result of non-selective excitation with an appropriate radio frequency pulse,[6] offers the possibility to probe Li(1)–Li(2) exchange processes via the temporal fluctuations of the electric quadrupolar interactions which the two Li ions experience at a given temperature. While in classical 1D or 2D exchange NMR spectroscopy local magnetic fields are used to label the Li spins,[11] in spin-

[a] B. Gadermaier, K. Hogrefe, Prof. Dr. H. M. R. Wilkening
Institute of Chemistry and Technology of Materials
Graz University of Technology
Stremayrgasse 9, 8010 Graz, Austria
E-mail: wilkening@tugraz.at
[b] Prof. Dr. P. Heitjans
Institute of Physical Chemistry and Electrochemistry
Leibniz University Hannover
Callinstraße 3–3a, 30167 Hannover, Germany

Supporting information for this article is available on the WWW under https://doi.org/10.1002/ejic.202000941

Part of the joint "German Chemical Society ADUC Prizewinner" Collection with EurJOC.

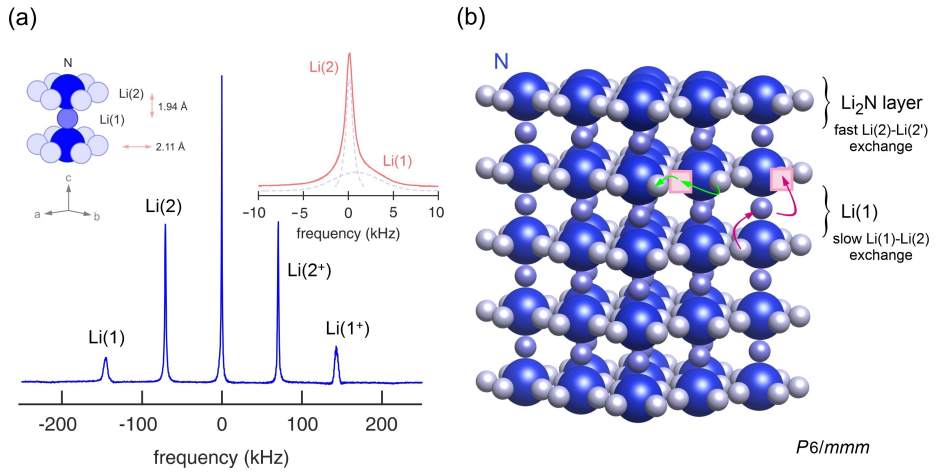

Figure 1. (a) ^{7}Li solid echo NMR spectrum of single crystalline Li_3N (77 MHz, 273 K; crystal orientation: $\boldsymbol{c} \parallel \boldsymbol{B}_0$). The inset shows a magnification of the two central lines representing the Li ions Li(1) and Li(2), the two pairs of satellites are marked by Li($i^{(+)}$) with $i = 1, 2$; see crystal structure. Dashed lines show a deconvolution of the overall single with a Gaussian line (Li(1)) and a Lorentzian line (Li(2)). The ratio of the respective areas is in agreement with the number densities of Li(1) and Li(2) in Li_3N. (b) Crystal structure of Li_3N (space group *P6/mmm*) showing the sequence of Li and Li_2N layers. Whereas fast Li^+ diffusion (Li(2)-Li(2′)) is present within the Li_2N layers, Li^+ exchange perpendicular to the c-axis (Li(1)–Li(2)) is slow.

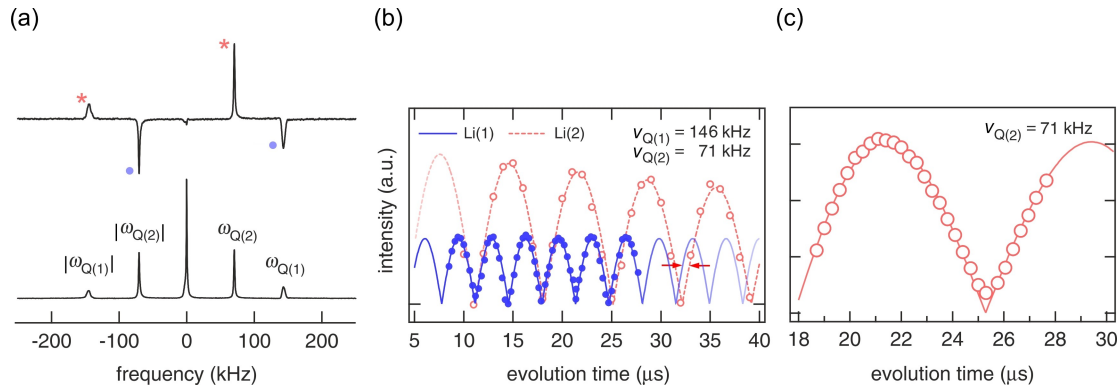

Figure 2. (a) Top: ^{7}Li NMR spin-alignment spectrum (77 MHz, $t_p = 13.8$ μs, $t_m = 10$ μs; crystal orientation: $\boldsymbol{c} \parallel \boldsymbol{B}_0$) recorded at 293 K; the corresponding pairs of satellite lines are marked by asterisks and dots, respectively. For comparison, a ^{7}Li NMR solid-echo spectrum is also shown, the interpulse delay was $t_e = 10$ μs. (b) Modulation of the satellite intensities belonging to Li(1) and Li(2) as a function of t_p; the signals labelled Li(1) and Li(2) in Figure 1a show the same behaviour as the signals Li(1^+) and Li(2^+). The lines show fits with a sinus function: $|\sin(\omega_{Q(1)}t_p)|$ yielding $\omega_{Q(1)}/2\pi = 145(3)$ kHz and $\omega_{Q(2)}/2\pi = 71(2)$ kHz in good agreement with the spectral values seen in (a). (c) Evolution of the Li(2) satellite line with higher data density in the range from $t_p = 18$ μs to $t_p = 28$ μs.

alignment echo NMR the quadrupole frequencies of the satellite lines are utilized to probe fluctuations on the kHz time scale. Hence, the method is sensitive to rather slow exchange rates that are usually not accessible by, *e.g.*, conventional NMR spin-lattice relaxation techniques or by pulsed field gradient (PFG) NMR methods (see Figure 2).[12] The latter techniques have, however, successfully been employed to study both the interlayer jump process and the intralayer jump process, which proceeds on much shorter length and time scales.[1d,h]

Here, we take advantage of a highly resolved single crystal ^{7}Li NMR spectrum of Li_3N[6] and used 1D SAE NMR to directly measure the Li(1)–Li(2) exchange rate close to room temperature. The method is similar to the ^{7}Li NMR selective inversion of both central lines[13] and satellite lines[14] but does, in the case of Li_3N, not suffer from too short dipolar NMR spin-lattice relaxation (T_1) times. For our purpose, we recorded ^{7}Li (quadrupolar) SAE NMR echoes via the three-pulse sequence introduced by Jeener and Broekaert.[12c,15] Fourier transformation revealed the generation of a pure quadrupolar spin-alignment state with the central lines being almost completely vanished at sufficiently low evolution times t_p.[6,16] We selectively blinded out one of the satellite lines by choosing the right evolution time and recorded its recovery as a function of mixing time t_m. The resulting buildup curve follows a single exponential and is solely controlled by the Li(1)–Li(2) hopping processes. Finally, we compare the SAE NMR jump rate with those published in literature earlier.[1i,6] Our study shows that it is indeed possible to selectively study an elementary diffusion process by 1D ^{7}Li SAE NMR with very high precision.

Although much more work on solid electrolytes is devoted to the finding of materials with exceptionally high Li^+ conduction properties, as these are needed to develop all-solid-

state (ceramic) batteries, the reliable determination of jump rates and diffusion coefficients is highly appreciated by computational chemists. They need appropriate data recorded with the necessary precision to develop and validate their diffusion models and to unravel the mechanism controlling cation exchange processes. In many cases, the different model substances, equipped with special properties in rather pure forms, build the basis to unveil the origins governing fast ion transport in solids.

Results and Discussion

The Jeener-Broekaert three-pulse sequence,[12c,15b,e,16–17] $90°_x - t_p - 45°_y - t_m - 45°_\varphi$, can be used to create spin-alignment order of an ensemble of quadrupolar nuclei that are subjected to electric quadrupole interactions of appropriate strength allowing for a non-selective excitation of the entire spectrum. If applied to the ^{7}Li NMR spectrum of Li_3N (300 K), shown in Figure 1a, the NMR response obtained after the reading pulse of the three-pulse sequence depends on the evolution time t_p ($t_m \rightarrow 0$) chosen. For the crystal orientation *c*-axis $\parallel \boldsymbol{B}_0$, with $\boldsymbol{B}_0$ being the orientation of the external magnetic field vector in the principle axis system, the amplitudes of the two pairs of satellite transitions appearing at ± 71 kHz (Li(2)) and at ± 146 kHz (Li(1)), respectively, are modulated according to $|\sin(\omega_{Q(i)} t_p)|$ with $i = 1,2$. In Figure 2b the absolute value of the signal amplitude is plotted against t_p. As $\omega_{Q(1)}/2\pi = \nu_{Q(1)} = \pm 146$ kHz is slightly larger than twice the quadrupole frequency of the Li(2) site ($\omega_{Q(1)}/\omega_{Q(2)} = 2.05$), we recognize a phase shift at sufficiently long evolution times t_p, as indicated by the horizontal arrows in Figure 2b.

By choosing an appropriate evolution time t_p we were able to selectively blank out one of the satellite signals belonging to Li(1). For instance, at $t_p = 14.5$ µs this signal does almost vanish, and the spin system is prepared to follow its recovery driven by Li^+ exchange process, that is, by fluctuations of $\omega_{Q(i)}$. A series of ^{7}Li spin-alignment spectra recorded at 318 K and fixed $t_p = 14.5$ µs but variable mixing time t_m (15 µs .. 1.5 ms) reveals that the originally suppressed signal indeed recovers. This recovery directly reflects the Li(1)–Li(2) interlayer cation exchange process as the Li^+ ions are subjected to quite different angular quadrupole frequencies with coupling constants in the kHz range. The recovery curve, which is obtained by plotting the normalized signal amplitude $S_{Li(1)}(t_p = \text{const.}, t_m)/S_0$ vs. t_m, is of pure exponential behaviour, see Figure 3b; S_0 refers to the amplitude at $t_m \rightarrow \infty$. Linearization of the curve (see inset of Figure 3) yields $\tau_{\parallel,318\,K} = 3.86 \times 10^{-3}$ s. The corresponding rate constant $\tau_\parallel^{-1} = 2519(190)$ s^{-1} is identified as the Li^+ exchange rate characterizing Li^+ exchange processes along the *c*-axis at 318 K. We can rule out interfering effects from spin-lattice relaxation on the buildup curve as the corresponding ^{7}Li NMR (quadrupolar) spin-lattice relaxation rate $1/T_{1Q,318\,K} = \tau_\parallel^{-1}$. Furthermore, as inferred from preliminary ^{6}Li NMR three-time stimulated echo experiments, see *e.g.*, Vogel and co-workers for an introduction into such type of experiments using ^{109}Ag,[18] the influence of any forward-backward jumps seem to be practically negligible; if present, they proceed on a shorter length scale. SAE NMR as carried out here is sensitive to a successful displacement of the Li ions as it is also sensed in direct current (DC) conductivity spectroscopy.[5b] Coming back to the recovery of the blanked out Li signal, the corresponding satellite is also affected by the exchange process, showing, as expected, a slight decrease in intensity followed by an increase due to spin-lattice relaxation at longer times.

Finally, we used the well-known Einstein-Smoluchowski equation, $D_\parallel = d_{ij}^2/(2g\tau_\parallel)$,[19] to convert this exchange rate into a Li^+ self-diffusion coefficient. As Li^+ diffusion proceeds along the *c*-axis, the geometry factor *g* was chosen to be $g = 1$. With the nearest neighbor distance d_{12} we obtained $D_\parallel = 1 \times 10^{-17}$ m^2 s^{-1}. $D_\parallel$, and thus $\tau_\parallel^{-1}$, agrees very well with jump rates deduced from ^{6}Li SAE NMR and ^{7}Li NMR. In the Arrhenius plot of Figure 4

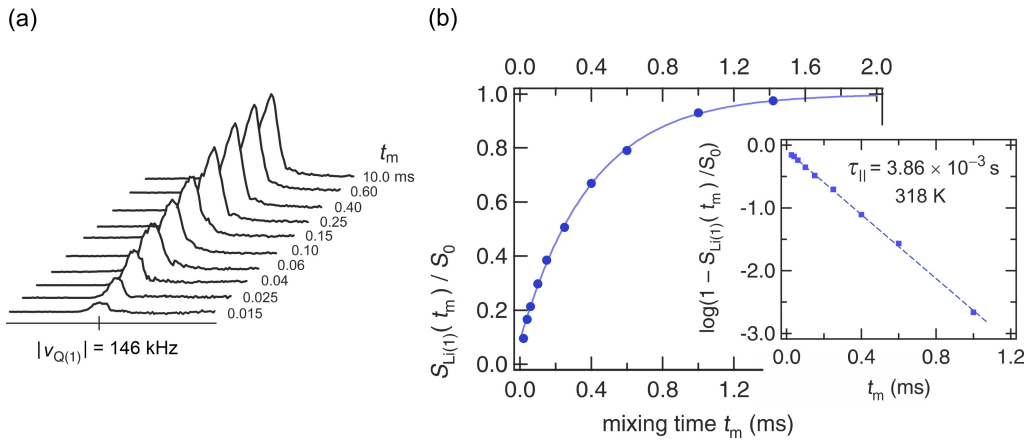

Figure 3. (a) ^{7}Li SAE NMR spectra recorded at $t_p = 14.5$ µs ($\omega_0/2\pi = 155$ MHz, 318 K; crystal orientation: $\boldsymbol{c} \parallel \boldsymbol{B}_0$) and for variable mixing times as indicated (0.015 ms $\leq t_m \leq$ 10 ms). The signal belongs to the satellite line of Li(1) appearing at a resonance frequency of 146 kHz. (b) Recovery of the normalized signal amplitude $S_{Li(1)}(t_p = 14.5$ µs, $t_m)/S_0$ shown in (a) as a function of t_m. The solid line represents a fit with an exponential function verified by the half-logarithmic plot (see inset). The dashed line shows a linear fit and yields a rate constant of $\tau_\parallel^{-1} = 2519(190)$ s^{-1} that characterizes the interlayer Li(1)–Li(2) diffusion in single crystalline Li_3N at 318 K.

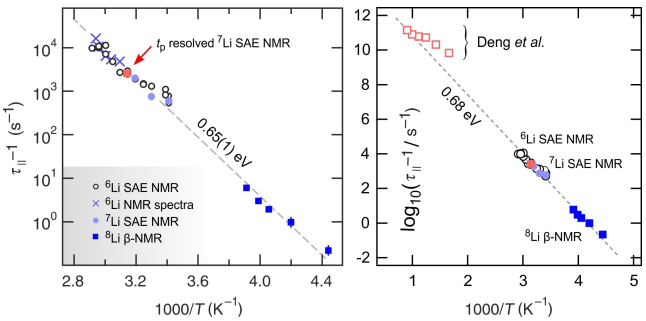

Figure 4. Left: Arrhenius plot showing the Li^+ jump rates deduced from various NMR methods used to characterize the interlayer jump process in Li_3N single crystals. Data taken from refs.[1i,6]. The jump rate directly measured by 1D evolution-time dependent ^{7}Li SAE perfectly agrees with the rates reported earlier. Altogether, the jump process was observed over a dynamic range of 5 decades. The dashed line shows a linear fit yielding an activation energy of 0.65(1) eV ($\tau_0^{-1} = 6.4\times10^{13}$ s^{-1}), which fully agrees with values reported in the literature by, for example, orientation-dependent conductivity measurements.[4,5b] Right: The same data as shown on the left, but also including the calculated values from Deng *et al.*[2b] by means of MD simulations. The dashed line reveals an activation energy of 0.68 eV; taken together, the rates span a dynamic range of approximately 12 decades.

the rates $\tau_{||}^{-1}$ ($=\tau_0^{-1}\exp(-E_{A,||}/(k_B T))$, k_B is Boltzmann's constant) from different NMR methods[1i,6] including also results from β-radiation detected ^{8}Li NMR[1o] are shown. The dashed line represents a linear fit that leads to an activation energy $E_{A,||}$ of 0.65(1) eV and a pre-exponential factor of $\tau_0^{-1} = 6.4\times10^{13}$ s^{-1}. The latter value agrees with the range typically measured for phonon frequencies in solids.[2b,20]

The activation energy probed by evolution-time resolved ^{7}Li SAE NMR ($E_{A,||} = 0.65(1)$ eV) is in perfect agreement with values deduced from PFG NMR performed by Brinkmann and co-workers (0.68(1) eV) at higher temperatures.[1d] It also agrees with that deduced from conductivity measurements carried out by Wahl (0.67(3) eV)[5b] robing long-range anisotropic Li ion transport in Li_3N. Table 1 gives an overview of earlier published activation energies and Arrhenius pre-factors characterizing the interlayer jump process in Li_3N single crystals. Unintentional H-doping may affect the dynamic properties. However, as pointed out by Wahl, the interlayer jump process is less affected by H centers.[5b] Here, as estimated via ^{1}H NMR (see also the Experimental Section), the concentration of H impurities turned out to be in the order of 10^{19} cm^{-3}, which is by a factor of ten lower than in the samples studied by Wahl (10^{20} cm^{-3}), belonging to the series of samples with a very low content of H.[5b]

Table 1. Activation energies $E_{A,||}$ and Arrhenius pre-factors obtained from both NMR methods and conductivity measurements being sensitive to long-range ion transport; data refer to Li_3N single crystals.

Method	$E_{A,||}$ (eV)	τ_0^{-1} (s^{-1})
^{7}Li NMR spin-lattice relaxation[a][1b]	0.62(3)	$\approx1\times10^{14}$
^{7}Li NMR central lines, quadrupole shift[1b]	0.68(8)	$7(4)\times10^{14}$
^{7}Li NMR line widths analysis[1h]	0.64(1)	2×10^{14}
^{7}Li PFG NMR[1d]	0.68(1)	$\approx1\times10^{14}$
^{8}Li β-NMR transients for (1)[1i]	0.57(3)	$1\times10^{12(0.5)}$
^{8}Li β-NMR ($1/T_1$ rates)[1i]	0.59(3)	$1\times10^{14(0.5)}$
conductivity measurements, $\sigma_{||}$[5b]	0.67(3)	$\approx1\times10^{14}$
conductivity measurements, $\sigma_{||}$[4a]	0.65	$\approx2.5\times10^{14}$

[a] Our own ^{7}Li NMR $1/T_1$ measurements on the present sample yielded 0.57(2) eV.

Recently published first-principle calculations focusing on the interlayer diffusion process yield activation energies of 0.47 eV for H-undoped Li_3N assuming that Li interstitials are the main charge carrier.[3] For H-doped Li_3N the activation energies for Li vacancies (0.75 eV) and Li interstitials (0.53 eV)[3] turned out to be larger but did not precisely match with experimental values. Quite recently, Deng *et al.* calculated diffusion coefficients $D_{||}$ and the activation energy of the interlayer jump process.[2b] A value of almost 0.6 eV has been calculated via molecular dynamics (MD) simulations using the Coulomb-Buckingham potential while the electrostatic spectral neighbor analysis potential (eSNAP) underestimates $E_{A,||}$ if one only considers a small temperature range.[2b] We converted $D_{||}$ into $\tau_{||}^{-1}$, the results are shown in Figure 4b. Altogether, good agreement is observed if we restrict the Arrhenius line (0.68 eV) to take only into account $D_{||}$ values calculated at the highest temperatures. Apart from this very recent study, the investigation by Sarnthein *et al.* using *ab initio* MD calculations taking advantage of the projector-augmented wave method remains one of the important calculations concerning Li^+ migration in Li_3N.[21] The study yields activation energies of 0.58 eV and 0.68 eV for interlayer Li jumps involving vacancies in the Li_2N planes.[21] The suggested knock-off diffusion mechanism, see Figure 5, is consistent with the principle of fluctuating quadrupole interactions ^{6,7}Li SAE NMR is based on.

Sarnthein *et al.* also calculated diffusion coefficients $D_{||}$ at 800 K.[21] Their value of 1.3×10^{-8} m^2 s^{-1} is in fair agreement with those from NMR spectroscopy if we extrapolate the Arrhenius line of Figure 4 toward higher temperatures. This extrapolation yields $\tau_{||}^{-1} = 1\times10^{10}$ s^{-1} at 800 K, which translates into a diffusion coefficient in the order of 0.4×10^{-9} m^2 s^{-1}. On the other hand, via eSNAP MD calculations Deng *et al.* reported a diffusion coefficient of 2×10^{-9} m^2 s^{-1} at 800 K.[2b] This value, despite the above mentioned underestimation of $E_{A,||}$, is in rather good agreement with jump rates deduced here. An even

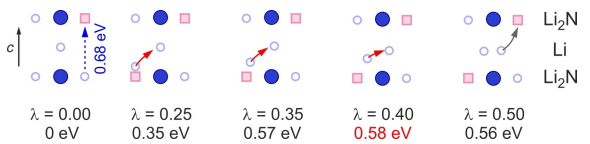

Figure 5. The interlayer Li^+ diffusion pathway suggested by Sarnthein *et al.* in Li_3N on the basis of ab initio MD calculations.[21] To fill the vacancy in the upper Li_2N layer, Li^+ moves parallel to the *c*-axis. The reaction coordinate λ describes the relative *z* coordinate of the Li ion that moves from the lower to the upper Li_2N plane. At $\lambda = 0.5$ it knocks off the Li(1) Li ion and the five configurations will repeat in reverse order according to a fully symmetric barrier. The pathway described by the five configurations, including the Li(1)–Li(2) exchange, is consistent with the underlying principle of ^{6,7}Li SAE NMR outlined above. The dashed arrow, that is, the almost parallel pathway to fill the Li_2N vacancy but bypassing the Li(1) site, would correspond to an activation energy of 0.68 eV, which would also be consistent with experimental data.

better agreement is found for diffusion coefficients calculated at higher temperature, see Figure 4b.

Summary and Conclusion

We used 1D (evolution-time resolved) ^{7}Li spin-alignment echo NMR to directly probe the slow Li(1)–Li(2) interlayer Li^+ jump process in Li_3N single crystals. According to the recovery of the blanked out Li(1) satellite line the interlayer exchange process is to be characterized by a jump rate of $2.5\times10^3\ s^{-1}$ (318 K). This rate perfectly agrees with those probed by alternative (time-domain) NMR methods including ^{6}Li SAE NMR[6] and ^{8}Li β-NMR[1i] revealing that around ambient conditions the mean activation energy of the Li(1)–Li(2) jump process is given by 0.65 eV. Together with the corresponding diffusion coefficient this value supports the vacancy-controlled knock-off diffusion mechanism previously suggested by Sarnthein *et al.*[21] In general, precisely measured dynamic parameters of small cations and anions are needed to validate diffusion models. The present study might stimulate computational chemists to reconsider Li_3N as a model system to investigate (slow) low-dimensional diffusion processes in crystalline solids.

Experimental Section

^{7}Li SAE NMR spectra and solid-echo spectra were recorded at Larmor frequencies $\omega_0/2\pi$ of 77 MHz (MSL 100 spectrometer, Bruker) and 155 MHz (MSL 400 spectrometer, Bruker) respectively. We used broadband probes to collect free induction decays and stimulated echoes as a function of temperature. The temperature in the sample chamber was adjusted with a flow of heated N_2 gas that we freshly evaporated. The temperature was monitored with an Oxford intelligent temperature controller (ITC) in combination with Ni–Cr-Ni thermocouples placed in the direct vicinity of the sample.

Li_3N single crystals were grown at the Max-Planck Institute for Solid State Research (Stuttgart), they were used in an earlier study for ^{6}Li SAE NMR experiments. The ruby-red single crystals (2 mm in thickness, 1 cm in length and 5 mm in width) were fire-sealed (under vacuum) in Duran® ampules to protect them permanently from any traces of moisture.

We employed the Jeener-Broekaert[15a,22] three pulse sequence $90^\circ_x-t_p-45^\circ_y-t_m-45^\circ_\varphi$ (see Figure S1, Supporting Information) to record ^{7}Li SAE NMR spectra as a function of both evolution time t_p and mixing time t_m. Extensive phase cycling,[15b,16a,23] see also the Supporting Information Table S1, was employed to pick out the correct phase coherence pathway for spin-3/2 nuclei and to suppress unwanted coherences. The 90° pulse length varied, depending on temperature and pulse power, from 2.0 to 2.8 μs. These values ensured a non-selective excitation of the entire spectrum. ^{1}H NMR measurements, using a Bruker Avance 500 spectrometer, were carried out to estimate the H content of our Li_3N single crystals with the help of a suitable reference sample (polycrystalline $LiBH_4$ and $LiBD_4$ with a known amount of H impurities); here the amount of H centres is estimated to not exceed the level of $10^{19}\ cm^{-3}$.

Acknowledgements

We thank the Deutsche Forschungsgemeinschaft for financial support in the frame of the research unit FOR1277 molife "Mobilität von Li–Ionen in Festkörpern" (WI3600 4–1 and 2-1). In addition, the study received funding from the European Union's Horizon 2020 research and innovation program under the grant agreement no. 769929. P.H. is grateful to the State of Lower Saxony (Germany) for the Niedersachsen Professorship "Mobility of Ions in Solids".

Conflict of Interest

The authors declare no conflict of interest.

Keywords: Diffusion · Electrochemistry · Lithium · Solid electrolytes · Spin-alignment echoes

[1] a) D. Brinkmann, M. Mali, J. Roos, R. Messer, *Solid State Ionics* **1981**, *5*, 409–412; b) D. Brinkmann, M. Mali, J. Roos, R. Messer, H. Birli, *Phys. Rev. B* **1982**, *26*, 4810–4825; c) D. Brinkmann, W. Freudenreich, J. Roos, *Solid State Commun.* **1978**, *28*, 233–237; d) E. Bechtold-Schweickert, M. Mali, J. Roos, D. Brinkmann, *Phys. Rev. B* **1984**, *30*, 2891–2893; e) U. v. Alpen, A. Rabenau, G. Talat, *Appl. Phys. Lett.* **1977**, *30*, 621–623; f) U. Alpen, *J. Solid State Chem.* **1979**, *29*, 379–392; g) M. F. Bell, A. Breitschwerdt, U. von Alpen, *Mater. Res. Bull.* **1981**, *16*, 267–272; h) R. Messer, H. Birli, K. Differt, *J. Phys. C* **1981**, *14*, 2731–2746; i) B. Bader, P. Heitjans, H.-J. Stöckmann, H. Ackermann, W. Buttler, P. Freiländer, G. Kiese, C. Van der Marel, A. Schirmer, *J. Phys. Condens. Matter* **1992**, *4*, 4779–4800; j) G. Hartley, L. Jin, B. Bergner, D. Spencer Jolly, G. Rees, S. Zekoll, Z. Ning, A. T. R. Pateman, C. Holc, P. Adamson, P. Bruce, *Chem. Mater.* **2019**, *31*; 9993–10001; k) N. Tapia-Ruiz, A. G. Gordon, C. M. Jewell, H. K. Edwards, C. W. Dunnill, J. M. Blackman, C. P. Snape, P. D. Brown, I. MacLaren, M. Baldoni, *Nat. Commun.* **2020**, *11*, 4492; l) W. Li, G. Wu, C. M. Araújo, R. H. Scheicher, A. Blomqvist, R. Ahuja, Z. Xiong, Y. Fengb, P. Chen, *Energy Environ. Sci.* **2010**, *3*, 1524–1530; m) H. Xu, Y. Li, A. Zhou, N. Wu, S. Xin, Z. Li, J. B. Goodenough, *Nano Lett.* **2018**, *18*, 7414–7418; n) A. S. Powell, J. S. Lord, D. H. Gregory, J. J. Titman, *J. Phys. Chem. C* **2009**, *113*, 20758–20763; o) P. Heitjans, *Solid State Ionics* **1986**, *18–9*, 50–64.

[2] a) A. Rabenau, *Solid State Ionics* **1982**, *6*, 277–293; b) Z. Deng, C. Chen, X.-G. Li, S. P. Ong, *npj Comp. Mater.* **2019**, *5*, 1–8; c) A. D. Mulliner, P. D. Battle, W. I. F. David, K. Refson, *Phys. Chem. Chem. Phys.* **2016**, *18*, 5605–5613.

[3] I. Kishida, F. Oba, Y. Koyama, A. Kuwabara, I. Tanaka, *Phys. Rev. B* **2009**, *80*, 024116.

[4] a) A. Hooper, T. Lapp, S. Skaarup, *Mater. Res. Bull.* **1979**, *14*, 1617–1622; b) T. Lapp, S. Skaarup, A. Hooper, *Solid State Ionics* **1983**, *11*, 97–103.

[5] a) J. Wahl, U. Holland, *Solid State Commun.* **1978**, *27*, 237–241; b) J. Wahl, *Solid State Commun.* **1979**, *29*, 485–490; c) B. Boukamp, R. Huggins, *Phys. Lett. A* **1976**, *58*, 231–233; d) B. Boukamp, R. Huggins, *Mat. Res. Bull.* **1978**, *13*, 23–32.

[6] M. Wilkening, D. Gebauer, P. Heitjans, *J. Phys. Condens. Matter* **2008**, *20*, 022201.

[7] P. Blaha, K. Schwarz, P. Herzig, *Phys. Rev. Lett.* **1985**, *54*, 1192–1195.

[8] B. Bader, P. Heitjans, H. Ackermann, P. Freilander, F. Fujara, G. Kiese, H. J. Stöckmann, C. Van der Marel, *Hyperfine Interact.* **1983**, *16*, 593–596.

[9] P. K. Burkert, H. P. Fritz, G. Stefaniak, *Z. Naturforsch. B* **1970**, *25*, 1220–1225.

[10] B. Bader, P. Heitjans, H. Ackermann, P. Freiländer, G. Kiese, A. Schirmer, H. J. Stöckmann, C. Van der Marel, *Ann. Phys.* **1985**, *42*, 169–174.

[11] a) J. Langer, D. L. Smiley, A. D. Bain, G. R. Goward, M. Wilkening, *J. Phys. Chem. C* **2016**, *120*, 3130–3138; b) P. Bottke, D. Freude, M. Wilkening, *J. Phys. Chem. C* **2013**, *117*, 8114–8119.

[12] a) M. Wilkening, P. Heitjans, *ChemPhysChem* **2012**, *13*, 53–65; b) B. Ruprecht, M. Wilkening, R. Uecker, P. Heitjans, *Phys. Chem. Chem. Phys.*

2012, *14*, 11974–11980; c) M. Wilkening, P. Heitjans, *J. Phys. Condens. Matter* **2006**, *18*, 9849–9862; d) Z. Wang, M. Gobet, V. Sarou-Kanian, D. Massiot, C. Bessada, M. Deschamps, *Phys. Chem. Chem. Phys.* **2012**, *14*, 13535–13538.

[13] L. J. M. Davis, B. L. Ellis, T. N. Ramesh, L. F. Nazar, A. D. Bain, G. R. Goward, *J. Phys. Chem. C* **2011**, *115*, 22603–22608.

[14] A. Kuhn, P. Heitjans, *Diff. Fundam.* **2010**, *12*, 97–99.

[15] a) P. Broekaert, J. Jeener, *Phys. Rev. B* **1977**, *15*, 4168–4173; b) F. Qi, G. Diezemann, H. Böhm, J. Lambert, R. Böhmer, *J. Magn. Reson.* **2004**, *169*, 225–239; c) R. Böhmer, K. R. Jeffrey, M. Vogel, *Prog. Nucl. Magn. Reson. Spectrosc.* **2007**, *50*, 87–174; d) M. Wilkening, C. Mühle, M. Jansen, P. Heitjans, *J. Phys. Chem. B* **2007**, *111*, 8691–8694; e) M. Wilkening, P. Heitjans, *Phys. Rev. B* **2008**, *77*, 024311.

[16] a) F. Qi, T. Jörg, R. Böhmer, *Solid State Nucl. Magn. Reson.* **2002**, *22*, 484–500; b) X. P. Tang, R. Busch, W. L. Johnson, Y. Wu, *Phys. Rev. Lett.* **1998**, *81*, 5358–5361; c) X. P. Tang, R. Busch, W. L. Johnson, Y. Wu, *Mater. Res. Soc. Symp. Proc.* **1999**, *554*, 87–92.

[17] a) R. Böhmer, T. Jörg, F. Qi, A. Titze, *Chem. Phys. Lett.* **2000**, *316*, 419–424; b) R. Böhmer, F. Qi, *Solid State Nucl. Magn. Reson.* **2007**, *31*, 28–34.

[18] C. Brinkmann, S. Faske, B. Koch, M. Vogel, *Z. Phys. Chem.* **2010**, *224*, 1535–1553.

[19] a) A. Einstein, *Ann. Phys.* **1905**, *322*, 549–560; b) M. von Smoluchowski, *Ann. Phys.* **1906**, *326*, 756–780.

[20] W. Kress, H. Grimm, W. Press, J. Lefebvre, *Phys. Rev. B* **1980**, *22*, 4620–4625.

[21] J. Sarnthein, K. Schwarz, P. E. Blöchl, *Phys. Rev. B* **1996**, *53*, 9084–9091.

[22] M. Lausch, H. W. Spiess, *J. Magn. Reson.* **1983**, *54*, 466–479.

[23] R. Böhmer, *J. Magn. Reson.* **2000**, *147*, 78–88.

Manuscript received: October 8, 2020
Revised manuscript received: January 13, 2021
Accepted manuscript online: January 14, 2021